

Sensitivity functions of spaceborne gravitational wave detectors for arbitrary time-delay interferometry combinations

Pan-Pan Wang¹, Yu-Jie Tan^{1,*}, Wei-Liang Qian^{2,3,†} and Cheng-Gang Shao^{1,‡}

¹*MOE Key Laboratory of Fundamental Physical Quantities Measurement, Hubei Key Laboratory of Gravitation and Quantum Physics, PGMF, and School of Physics, Huazhong University of Science and Technology, Wuhan 430074, People's Republic of China*
²*Escola de Engenharia de Lorena, Universidade de São Paulo, 12602-810 Lorena, SP, Brazil*
³*Center for Gravitation and Cosmology, College of Physical Science and Technology, Yangzhou University, 225009 Yangzhou, China*



(Received 16 December 2020; accepted 22 February 2021; published 17 March 2021)

The principal aim of the space-based gravitational wave detectors is to explore the gravitational waves in the 0.1 mHz-1 Hz frequency band. To maximize the potential capability of the experimental apparatus regarding the instrument performance, one needs to acquire accurate information on its sensitivity limit. The sensitivity curve in question, by definition, depends on the amplitudes of signal and noise involved in the measurement. In this work, we explicitly derive, under rather universal assumptions irrelevant to the detailed form of the time-delay interferometry combination, general results of the sensitivity functions. The key feature of the present approach is that both the all-sky and polarization average can be factorized and henceforth evaluated analytically. The resultant expressions are then applied to a variety of time-delay interferometry combinations, inclusively for the optimal channels. In particular, the asymptotical forms of the sensitivity functions are obtained at the high and low frequency limits, and the subsequential implications are analyzed. When compared with the approaches in terms of numerical integration, the obtained formulism furnishes a more straightforward as well as efficient access to the relevant signal noise ratios for the spaceborne gravitational wave detectors.

DOI: [10.1103/PhysRevD.103.063021](https://doi.org/10.1103/PhysRevD.103.063021)

I. INTRODUCTION

As first predicted by general relativity, the gravitational waves (GWs) are ripples in the fabric of spacetime, triggered by accelerated masses. The resultant disturbances propagate in the waveform at the speed of light while transporting energy, referred to as gravitational radiation. Preceded by various indirect detections, the first direct evidence for the existence of GW was reported by the LIGO Scientific Collaboration and the Virgo Collaboration through a series of measurements initiated in 2015 [1–7]. Such an experimental triumph unfolds a novel possibility, besides those in terms of electromagnetic radiations, for observing the Universe. In particular, it serves to attest to the validity of other candidate theories of gravity, particularly in the strong-field regime. Inspired by the achievement, and motivated by its significant further potential, a variety of related ground-based as well as spaceborne projects, also based on the laser interferometers, have been subsequently carried out [8–18]. The ground-based detectors, such as Advanced LIGO [8], Advanced Virgo [9], and

KAGRA [15], are largely aimed at the high-frequency band (10–10⁴ Hz). On the other hand, the spaceborne ones, which consists of LISA [11], TianQin [13] and TaiJi [14], probe GWs in the frequency band of millihertz meanwhile, DECIGO [10] operates in the frequency band of 0.1 to 10 Hz.

To determine whether the detector is capable to observe GWs emanated from a particular source, it is crucial to acquire the sensitivity limit of the instrument [19–22]. Typically, the sensitivity of the detector can be quantified by the ratio of the source strength to the instrument noise. This is referred to in the literature as the signal-noise ratio (SNR), often presented in the frequency domain. On the one hand, in order to improve the SNR, one strives to suppress various types of noises, encountered in the laser interferometric measurements. For instance, the noise due to the laser frequency fluctuations, subjected to an unknown temporal form, is usually more significant than those of other origins by several orders of magnitude [23]. For the ground-based interferometers, it is feasible to tune the two armlengths to be precisely identical so that its cancelation can be implemented more straightforwardly. For space-based GW detectors, however, the spatial layout of the experimental setup is more extensive, and

*yjtan@hust.edu.cn

†wlqian@usp.br

‡cgshao@hust.edu.cn

furthermore, the movements of the spacecrafts are governed by the revolution orbits. As a result, it becomes impossible for space-based detectors to maintain constant armlengths. Consequently, the laser phase noises through different arms may experience different time-delays, and cannot be canceled out intuitively. In this regard, the time-delay interferometry (TDI) technique introduces virtual equal arm interferometric measurements in order for the laser frequency fluctuations to be canceled out [23,24]. In the literature, various TDI combinations have been proposed and extensively investigated [25–27]. Those combinations have been shown to efficiently cancel out the laser noise and some particular combinations might be preferable for specific merger systems. Nonetheless, several other minor sources remain inevitable and consequently constitute the setup noise floor. For LISA and TianQin, the latter largely consists of contributions from the acceleration and shot noises. In the present study, we will consider various TDI combinations that suppress the noise down to the level governed by the above inevitable noise sources.

On the other hand, the sensitivity curve of a detector also depends on the properties of the physical system from which the GWs are emanated. To be specific, the response function is governed by the information regarding the specific merger process, the polarization states of the GW, the orientation of the source to the detector, and the relevant layout of the detector. Here, the strength of the source can be expressed in terms of the strain spectral density. For unspecified GW sources, the orientation of the binary merger in terms of the all-sky solid angle as well as all possible polarization states are usually averaged out by the end of the calculations. Technically, it is not trivial to perform the above angular average analytically, and much effort has been developed to this topic. For spaceborne GW interferometers, semianalytic calculations were presented for the averaged response functions, and the results had been simplified to expressions containing unsolved definite integrals [19]. For the Michelson TDI combinations [28], a similar approach gave rise to resultant expressions involving the sum of definite integrals, and the results are then extended to and all six TDI combinations [29]. By employing the Monte Carlo simulation, the average regarding the source orientations and polarization angles were carried out [30,31]. Nonetheless, fully analytical expressions for the Michelson TDI combinations were successfully obtained in [32]. The purpose of the present work is to further generalize the above study by deriving full analytical expressions for all existing TDI combinations. In particular, as demonstrated below, for arbitrary TDI combination, the angular average of the all-sky solid angle as well as the polarization states can be factorized. Subsequently, the relevant integrations are well-defined and can be performed analytically. Based on the obtained results, we proceed to investigate the asymptotical properties of the averaged response function for specific TDI

combinations. Moreover, the optimal expressions for particular TDI combinations are derived.

The paper is organized as follows. In Sec. II, we first give a brief review of the TDI algorithm for the cancelation of the laser phase noises and then discuss the antenna response function. By employing the detector frame, in Sec. III, the formulae for sensitivity functions are derived for any given TDI combination. The asymptotic behaviors of a few relevant TDI combinations are further analyzed and discussed in Sec. IV. The concluding remarks are given in Sec. V. A detailed account of derivations is delegated to the Appendixes. In Appendix A, we list the polynomials of delay operators of all TDI combinations included in the present study. The calculations, inclusively the integration regarding all-sky angle and polarization average, are presented in Appendix B.

II. NOISE SOURCES AND RESPONSE FUNCTION FOR TIME-DELAY INTERFEROMETRY COMBINATIONS

The spaceborne GW detection is realized through laser interferometry. In order to maximize the observable effect, a laser beam emanated from a *remote* spacecraft (SC) is directed to interfere with that from the *local* SC. The spacetime distortion owing to the presence of GW is expected to introduce an additional phase shift. Such a signal is added up to the background ones inclusively amid various types of noises. The latter might even be orders of magnitude larger than the primary signal of interest. In practice, the measurements are recorded in terms of the fractional Doppler shift. As mentioned above, the noises also inevitably play a significant part in the above-mentioned Doppler shift and have to be suppressed at least below the magnitude of GW signals. In this section, we will focus on the estimation of the noise terms for TDI combinations and the derivation of the general form of

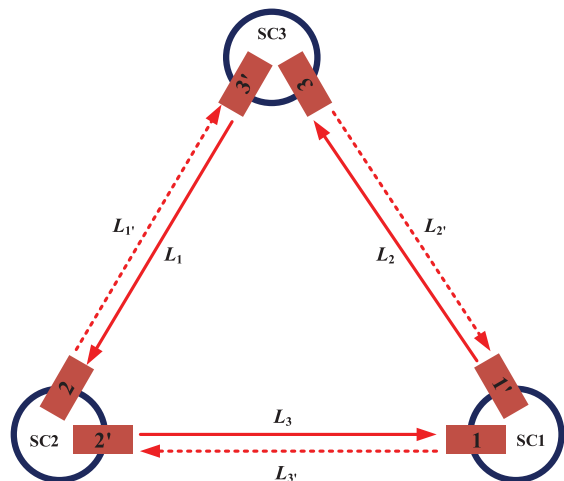


FIG. 1. The experimental layout of the space-based laser interferometry consists of laser sources and links.

the GW response function for spaceborne detectors. The experimental setup of a spaceborne detector is illustrated in Fig. 1. It consists of three identical SC approximately forming a triangle. Consequently, the effective armlength of the interferometer extends over 10^5 – 10^6 kilometers. Although the armlengths are inevitably time-varying, the chosen orbits are aimed to maintain the constellation as “rigid” as possible. The resultant configuration keeps a small variation within 1% for each detector armlength.

In the present work, we follow the notations utilized in Ref. [24]. For each SC, two optical benches (OBs) are installed, each of which houses a test mass (TM) acting as an inertial sensor. The two OBs aboard the i th SC are labeled by i, i' . As shown in Fig. 1, the optical path linking the other two SC on the opposite side of the i th SC is

$$\begin{aligned}\eta_i(t) &= h_i(t) + \mathcal{D}_{i-1}p_{i+1}(t) - p_i(t) + \vec{n}_{i-1}[\mathcal{D}_{i-1}\vec{\delta}_{(i+1)'}(t) - \vec{\delta}_i(t)] + N_i^{\text{opt}}(t), \\ \eta_{i'}(t) &= h_{i'}(t) + \mathcal{D}_{(i+1)'}p_{i-1}(t) - p_i(t) + \vec{n}_{i+1}' \cdot [\vec{\delta}_{i'}(t) - \mathcal{D}_{(i+1)'}\vec{\delta}_{i-1}(t)] + N_{i'}^{\text{opt}}(t).\end{aligned}\quad (1)$$

These observables are directly related to the photon paths. To be more specific, η_i (or $\eta_{i'}$) indicates the measured Doppler shift involving the photon propagation along the detector arm L_{i-1} ($L_{(i+1)'}$) in the counterclockwise (clockwise) direction. The GW signals $h_i(t)$ and $h_{i'}(t)$ are incorporated into the optical path length, which will be discussed in detail below in Sec. II B. The time delay operations, $\mathcal{D}_i, \mathcal{D}_{i'}$, are defined as $\mathcal{D}_j f(t) = f(t - \frac{L_j(t)}{c})$ with c being the speed of light. These quantities are associated with the corresponding detector arms $L_i, L_{i'}$, owing to the time consumed during which the photon traverses the detector arm. The laser phase noises in i th OB are denoted by $p_i(t)$, and $\vec{\delta}_i$ is the mechanical fluctuations induced by the random velocity noises of the TM. N_i^{opt} and $N_{i'}^{\text{opt}}$ are the fluctuations due to shot noises. In order to reduce the noises $p_i(t)$, one further introduces linear combinations of η_i , as will be discussed in the following subsection.

denoted by $L_i(L_{i'})$. Here, one adopts the convention that the light paths $L_1 \rightarrow L_2 \rightarrow L_3$ ($L_{1'} \rightarrow L_{2'} \rightarrow L_{3'}$) form a counterclockwise (clockwise) circulation. The optical paths connecting the six OBs give rise to a total of six laser links, through which the interferometric measurements are performed between the local and remote laser beams. To be more specific, there are four types of data streams, namely, the science interferometric measurements, test mass measurements, reference measurements, and sideband measurements. Among other minor sources of noises, for simplicity, we will only consider explicitly those due to the laser phase fluctuations, test mass mechanical vibrations, and shot noises. It is convenient to introduce intermediate variables, $\eta_i, \eta_{i'}$ as follows [33]:

A. Time-delay interferometry and noise cancellation

The TDI algorithm makes use of linear combinations of the intermediate observables $\eta_i, \eta_{i'}$ defined in Eq. (1). The aim of the approach is that the resultant quantities will be laser noise free. Such combinations are expressed in terms of polynomials of the delay operators [34], namely,

$$\text{TDI} = \sum_{i=1}^3 (P_i \eta_i + P_{i'} \eta_{i'}). \quad (2)$$

To encounter the proper coefficients of the polynomials, one may transfer the problem into that of finding the module of syzygies. The latter, in turn, can be resolved by evaluating the Grobner basis for the ideal generated by the coefficients appearing in the constraint, and then use it to construct the generating set for the module. The detail of the above procedure can be found in [24]. By employing the combinations, the resultant power spectral densities (PSDs) of the remaining noises, namely, the TM and shot noises, read

$$S_{\text{TDI}^a}(\Omega) = S_{\text{pf}}(\Omega) \sum_{i=1}^3 [|\tilde{P}_i(\Omega) + \tilde{P}_{(i+1)' }(\Omega)\tilde{D}_{(i-1)' }(\Omega)|^2 + |\tilde{P}_i(\Omega)\tilde{D}_{i-1}(\Omega) + \tilde{P}_{(i+1)' }(\Omega)|^2], \quad (3)$$

and

$$S_{\text{TDI}^{\text{shot}}}(\Omega) = S_{\text{opt}}(\Omega) \sum_{i=1}^3 [|\tilde{P}_i(\Omega)|^2 + |\tilde{P}_{i'}(\Omega)|^2], \quad (4)$$

where Ω is the observed frequency, and \tilde{D}_i is the Fourier transform of the time-delay operator. The dimensionless

$S_{\text{pf}} = \frac{s_a^2}{(\Omega c)^2}$ and $S_{\text{opt}} = \frac{\Omega^2 s_x^2}{c^2}$ measure the relative PSD of TM and shot noises, where s_a, s_x are the respective amplitude spectral densities (ASDs).

As the TM and shot noises originate from different physical natures, they are treated as independent variables [35,36]. The total noise PSD thus can be written as

$$\begin{aligned} N(u) &= S_{\text{TDI}^a}(u) + S_{\text{TDI}^{\text{shot}}}(u) \\ &= C_1[\tilde{P}_i(u)]n_1(u) + 4C_2[\tilde{P}_i(u)]n_2(u), \end{aligned} \quad (5)$$

where coefficients

$$\begin{aligned} C_1[\tilde{P}_i(u)] &= \sum_{i=1}^3 \text{Re}[|\tilde{P}_i|^2 + |\tilde{P}_{i'}|^2], \\ C_2[\tilde{P}_i(u)] &= \sum_{i=1}^3 \text{Re}[\tilde{P}_i \tilde{P}_{(i+1)'}^*], \end{aligned} \quad (6)$$

and

$$\begin{aligned} n_1(u) &= 2S_{\text{pf}} + S_{\text{opt}}, \\ n_2(u) &= S_{\text{pf}} \cos u, \end{aligned} \quad (7)$$

where one assumes that all of the armlengths are equal, the Fourier transform of the delay operator possess the form $\tilde{D}_i = e^{i\frac{\Omega L}{c}}$, and defines $u = \frac{\Omega L}{c}$ as a dimensionless quantity.

For the spaceborne GW detection, different data combinations may produce different link configurations. In practice, there are a variety of TDI combinations, in terms of eight-link observables: unequal-arm Michelson X , Relay U , beacon P and monitor E of first-generation TDI, and six-link observables: Sagnac α , fully symmetrized Sagnac ζ of first-generation TDI [26]. In Appendix A, we enumerate the coefficients of the polynomials $P_i, P_{i'}$ of these combinations, while most of the following derivations are based on rather general footing.

For illustration purpose, in the remainder of the manuscript, when referring to an explicit example, we will always consider the first-generation TDI Michelson combination X_1 . To be specific, the coefficients of the X_1 are given by

$$\begin{aligned} P_1 &= (\mathcal{D}_{2'2} - 1), P_2 = 0, P_3 = (\mathcal{D}_{2'} - \mathcal{D}_{33'2'}), \\ P_{1'} &= (1 - \mathcal{D}_{33'}), P_{2'} = (\mathcal{D}_{2'23} - \mathcal{D}_3), P_{3'} = 0. \end{aligned} \quad (8)$$

By combining Eqs. (5) and (8), the PSD for total noises (TM acceleration noises and shot noises) for the first-generation Michelson combination is given by

$$N_{X_1}(u) = \frac{s_a^2 L^2}{u^2 c^4} (8 \sin^2 2u + 32 \sin^2 u) + 16 \frac{u^2 s_x^2}{L^2} \sin^2 u. \quad (9)$$

B. Gravitational wave response function

As the GWs traverse through the vicinity of the spaceborne detector, the subsequential distortions of the

spacetime curvature will be recorded as Doppler shifts in the laser frequency. Subsequently, the optical path length of a photon emitted by one SC and received by another is modified. It can be estimated by evaluating the photon's geodesic. Let us consider a laser beam emanated at $t = t_1$ from the position $\vec{r}_A = \vec{r}(t_1)$, which is eventually received at $\vec{r}_B = \vec{r}(t_2)$ at $t = t_2$. The corresponding optical path length is $L = c(t_2 - t_1)$. From the viewpoint of an observer located in the background flat spacetime, the position vector of the beam at moment t can be expressed as $\vec{r}(t) \equiv \vec{r}_A + c(t - t_1)\hat{n}$, where \hat{n} indicates the direction of the photon propagation. To the first-order approximation, one may estimate the small variation of the time interval due to the metric perturbation introduced by the GW.

The world line of a photon has a null line element

$$0 = ds^2 = -c^2 dt^2 + dx^2 + dy^2 + dz^2 + h_{ij} dx^i dx^j. \quad (10)$$

Here, the indices i, j run over spatial ones only, and $dx^i = n^i d\lambda$, λ measures the Euclidean length. The components of the metric perturbation are denoted by h_{ij} . We introduce the scalar function

$$h(t) \equiv h_{ij} n^i n^j = h_+(t) \xi_+ + h_\times(t) \xi_\times, \quad (11)$$

where h_+ and h_\times are the amplitudes of two GW polarization states, determined by the specific merger system. ξ_+ and ξ_\times are known as the direction functions, defined by the contractions between the tensorial basis (for the plus or cross modes) and $\hat{n} \hat{n}$. The tensorial basis is conveniently expressed in terms of the unit vectors determined by the orientation of the GW source. Moreover, the polar angles on the celestial sphere, $(\hat{\theta}, \hat{\phi})$, are chosen so that they form a set of orthonormal basis vectors, when complemented by \hat{w} , the direction of wave propagation. Therefore, the direction functions can be expressed using the above angular variables as

$$\begin{aligned} \xi_+ &= (\hat{\theta} \cdot \hat{n})^2 - (\hat{\phi} \cdot \hat{n})^2, \\ \xi_\times &= 2(\hat{\theta} \cdot \hat{n})(\hat{\phi} \cdot \hat{n}). \end{aligned} \quad (12)$$

Based on above notation, one can show [37] that the relative Doppler shift of the laser beam along one arm in the time domain.

$$\frac{\delta\nu(t)}{\nu_0} = \frac{-1}{2(1 - \hat{k} \cdot \hat{n})} \left[h \left(t - \hat{k} \cdot \frac{\vec{r}_B}{c} \right) - h \left(t - \hat{k} \cdot \frac{\vec{r}_A}{c} - \frac{L}{c} \right) \right]. \quad (13)$$

By performing the Fourier transform, one can rewrite the above result in the frequency domain as follows

$$\frac{\delta\nu(\Omega)}{\nu_0} = \frac{h(\Omega)}{2(1 - \hat{k} \cdot \hat{n})} e^{i\Omega \frac{L + k\tau_A}{c}} [1 - e^{-i\Omega L(1 - \hat{k} \cdot \hat{n})}], \quad (14)$$

It is convenient to separate the plus and cross modes by substituting Eq. (11) into Eq. (14), one finds

$$\frac{\delta\nu(\Omega)}{\nu_0} = F_+(\Omega)h_+(\Omega) + F_\times(\Omega)h_\times(\Omega) \quad (15)$$

where F_+ and F_\times are governed by the specific detector layout regarding the two polarization states and are known as the response functions.

$$\begin{aligned} F_{+, \times} &= \sum_{i=1}^3 \tilde{P}_i F_{\eta_i; +, \times} + \tilde{P}_{i'} F_{\eta_{i'}; +, \times} \\ &= \tilde{P}_1 \frac{e^{i\Omega L_3(1 + \hat{w} \cdot \hat{n}_3)/c}}{2(1 + \hat{w} \cdot \hat{n}_3)} [1 - e^{-i\Omega L_3(1 + \hat{w} \cdot \hat{n}_3)/c}] \xi_{3; +, \times} + \tilde{P}_2 \frac{e^{i\Omega L_1(1 - \hat{w} \cdot \hat{n}_2)/c}}{2(1 + \hat{w} \cdot \hat{n}_1)} [1 - e^{-i\Omega L_1(1 + \hat{w} \cdot \hat{n}_1)/c}] \xi_{1; +, \times} \\ &\quad + \tilde{P}_3 \frac{e^{i\Omega L_2/c}}{2(1 + \hat{w} \cdot \hat{n}_2)} [1 - e^{-i\Omega L_2(1 + \hat{w} \cdot \hat{n}_2)/c}] \xi_{2; +, \times} + \tilde{P}_{1'} \frac{e^{i\Omega L_2(1 - \hat{w} \cdot \hat{n}_2)/c}}{2(1 - \hat{w} \cdot \hat{n}_2)} [1 - e^{-i\Omega L_2(1 - \hat{w} \cdot \hat{n}_2)/c}] \xi_{2; +, \times} \\ &\quad + \tilde{P}_{2'} \frac{e^{i\Omega L_3/c}}{2(1 - \hat{w} \cdot \hat{n}_3)} [1 - e^{-i\Omega L_3(1 - \hat{w} \cdot \hat{n}_3)/c}] \xi_{3; +, \times} + \tilde{P}_{3'} \frac{e^{i\Omega L_1(1 + \hat{w} \cdot \hat{n}_1)/c}}{2(1 - \hat{w} \cdot \hat{n}_1)} [1 - e^{-i\Omega L_1(1 - \hat{w} \cdot \hat{n}_1)/c}] \xi_{1; +, \times}. \end{aligned} \quad (17)$$

In practice, both the orientation of the GW source and the polarization angle are largely unknown to us ahead of any detection. These angular degrees of freedom will be averaged out in the calculation of the response function. In the following section, we will deal with specific detector layout and derive the desired analytical expressions for the averaged response functions.

III. THE AVERAGED RESPONSE FUNCTION OF SPACEBORNE GRAVITATIONAL WAVE DETECTORS

A. The detector frame

To calculate the averaged response function, we consider the detector Cartesian coordinate system in terms of $(\hat{e}_x, \hat{e}_y, \hat{e}_z)$. One places the coordinate origin at the location of SC1. The x - y plane is chosen to coincide with the triangle detector plane, where \hat{e}_x equally divide the angle formed by the rays SC1-SC2 and SC1-SC3 as illustrated in Fig. 2.

The position vectors and unit vectors of the three SC can be written as

$$\begin{aligned} \vec{r}_1 &= (0, 0, 0), \\ \hat{n}_1 &= (0, 1, 0), \\ \vec{r}_2 &= -L\hat{n}_3 = L\left(\cos\frac{\gamma}{2}, \sin\frac{\gamma}{2}, 0\right), \\ \vec{r}_3 &= L\hat{n}_2 = L\left(\cos\frac{\gamma}{2}, -\sin\frac{\gamma}{2}, 0\right). \end{aligned} \quad (18)$$

For instance, the response functions for the observables $\eta_1, \eta_{1'}$ associated with the arm $L_3, L_{2'}$ are written as

$$\begin{aligned} F_{\eta_1, +, \times}(\Omega) &= \frac{e^{i\Omega L_3(1 + \hat{w} \cdot \hat{n}_3)/c}}{2(1 + \hat{w} \cdot \hat{n}_3)} [1 - e^{-i\Omega L_3(1 + \hat{w} \cdot \hat{n}_3)/c}] \xi_{3; +, \times}, \\ F_{\eta_{1'}, +, \times}(\Omega) &= \frac{e^{i\Omega L_2(1 - \hat{w} \cdot \hat{n}_2)/c}}{2(1 - \hat{w} \cdot \hat{n}_2)} [1 - e^{-i\Omega L_2(1 - \hat{w} \cdot \hat{n}_2)/c}] \xi_{2; +, \times}. \end{aligned} \quad (16)$$

Subsequently, for an arbitrary TDI combination given by Eq. (2), the corresponding response function should be evaluated according to the specific light route and combination which gives

In practical calculations, another two coordinate systems [39–41] are often involved: the observational reference frame (ORF) $(\hat{\theta}, \hat{\phi}, \hat{w})$ (already defined above) and the canonical reference frame (CRF) $(\hat{p}, \hat{q}, \hat{w})$. The ORF frame measures the orientation of the source in terms of the polar angles on the celestial sphere. We choose the sign of \hat{w} so that

$$\hat{w} \equiv -\hat{k} = \sin\theta \cos\phi \hat{e}_x + \sin\theta \sin\phi \hat{e}_y + \cos\theta \hat{e}_z. \quad (19)$$

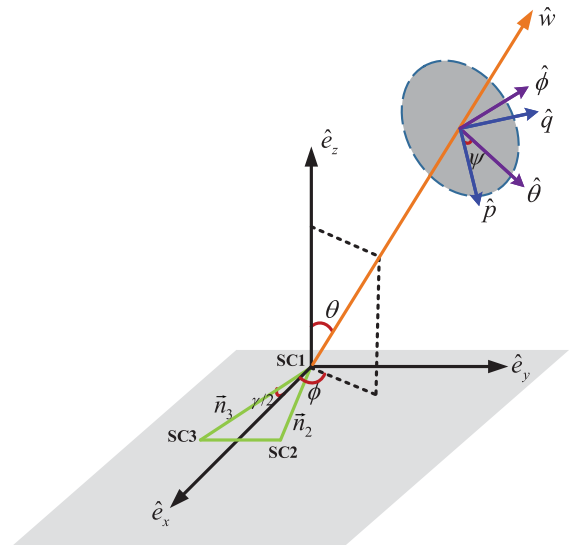


FIG. 2. The detector frame [38] defined in terms of $(\hat{e}_x, \hat{e}_y, \hat{e}_z)$.

Thus the coordinate system is right-hand oriented as $\hat{w} = \hat{\theta} \times \hat{\phi}$ and

$$\begin{aligned}\hat{\theta} &\equiv \partial\hat{w}/\partial\theta = \cos\theta \cos\phi \hat{e}_x + \cos\theta \sin\phi \hat{e}_y - \sin\theta \hat{e}_z, \\ \hat{\phi} &\equiv \partial\hat{w}/(\sin\theta\partial\phi) = -\sin\phi \hat{e}_x + \cos\phi \hat{e}_y.\end{aligned}\quad (20)$$

The CRF frame is more appropriate to describe the polarization state, which can be obtained by simply rotating ORF about the \hat{w} axis by an angle ψ clockwise. The two resultant unit vectors \hat{p} and \hat{q} are

$$\begin{aligned}\hat{p} &= \cos\psi \hat{\theta} - \sin\psi \hat{\phi} \\ \hat{q} &= \sin\psi \hat{\theta} + \cos\psi \hat{\phi}.\end{aligned}\quad (21)$$

Apparently, a GW signal propagating along \hat{k} can be equivalently written in ORF and CRF as

$$\vec{h}(t) \equiv h_{\text{CRF}+}(t)\epsilon^+ + h_{\text{CRF}\times}(t)\epsilon^\times = h_+(t)\epsilon^+ + h_\times(t)\epsilon^\times.\quad (22)$$

Here the tensorial bases in the two reference frames are $\epsilon^+ \equiv \hat{p} \otimes \hat{p} - \hat{q} \otimes \hat{q}$, $\epsilon^\times \equiv \hat{p} \otimes \hat{q} + \hat{p} \otimes \hat{q}$, and $e^+ = \hat{\theta} \otimes \hat{\theta} - \hat{\phi} \otimes \hat{\phi}$, $e^\times = \hat{\theta} \otimes \hat{\phi} + \hat{\phi} \otimes \hat{\theta}$. They are related to each other due to Eq. (21). The coefficients $h_{\text{CRF}+}(t)$, $h_{\text{CRF}\times}(t)$, $h_+(t)$, $h_\times(t)$ are the corresponding GW amplitudes.

In the frequency domain, the amplitudes for a monochromatical GW source can be written as [42]

$$\begin{aligned}h_+(\Omega) &= H \left(\frac{1 + \cos^2 \iota}{2} \cos 2\psi + i \cos \iota \sin 2\psi \right), \\ h_\times(\Omega) &= H \left(-\frac{1 + \cos^2 \iota}{2} \sin 2\psi + i \cos \iota \cos 2\psi \right),\end{aligned}\quad (23)$$

where ι is the inclination angle of source orbital plane with respect to the $\hat{p} - \hat{q}$ plane. H is known as the GW strain, determined by the specific merger system.

In the detector frame, one may write down the explicit forms of the direction functions Eq. (12) as follows

$$\begin{aligned}\xi_{1,+} &= \cos^2\theta \sin^2\phi - \cos^2\phi, \\ \xi_{2,+} &= \cos^2\theta \cos^2\tilde{\phi} - \sin^2\tilde{\phi}, \\ \xi_{3,+} &= \cos^2\theta \cos^2\tilde{\phi} - \sin^2\phi,\end{aligned}\quad (24)$$

and

$$\begin{aligned}\xi_{1,\times} &= \cos\theta \sin 2\phi, \\ \xi_{2,\times} &= -\cos\theta \sin 2\tilde{\phi}, \\ \xi_{3,\times} &= -\cos\theta \sin 2\tilde{\phi}.\end{aligned}\quad (25)$$

Also, we have

$$\begin{aligned}\hat{w} \cdot \hat{n}_1 &= \sin\theta \sin\phi, \\ \hat{w} \cdot \hat{n}_2 &= \sin\theta \cos\tilde{\phi}, \\ \hat{w} \cdot \hat{n}_3 &= -\sin\theta \cos\phi\end{aligned}\quad (26)$$

with $\phi = \phi - \frac{\gamma}{2}$, $\tilde{\phi} = \phi + \frac{\gamma}{2}$, and in this paper we take $\gamma = \frac{\pi}{3}$.

To evaluate the PSD of the GW signal, one proceeds to calculate the square of Eq. (17), which gives

$$\begin{aligned}4|F_{+,\times}|^2 &= |a|^2(\xi_{3;+,\times})^2 + |b|^2(\xi_{1;+,\times})^2 + |c|^2(\xi_{2;+,\times})^2 + 2\text{Re}(ab^*)\xi_{3;+,\times}\xi_{1;+,\times} + 2\text{Re}(ac^*)\xi_{3;+,\times}\xi_{2;+,\times} \\ &\quad + 2\text{Re}(bc^*)\xi_{1;+,\times}\xi_{2;+,\times},\end{aligned}\quad (27)$$

where

$$\begin{aligned}a &= \tilde{P}_1 e^{-iu \sin\theta \cos\phi} \frac{1 - e^{-iu(1 - \sin\theta \cos\phi)}}{1 - \sin\theta \cos\phi} + \tilde{P}_2 e^{-iu(1 + \sin\theta \cos\phi)} \frac{1 - e^{-iu(1 + \sin\theta \cos\phi)}}{1 + \sin\theta \cos\phi}, \\ b &= \tilde{P}_2 e^{-iu \sin\theta \cos\tilde{\phi}} \frac{1 - e^{-iu(1 + \sin\theta \sin\phi)}}{1 + \sin\theta \sin\phi} + \tilde{P}_3 e^{-iu \sin\theta \cos\phi} \frac{1 - e^{-iu(1 - \sin\theta \sin\phi)}}{1 - \sin\theta \sin\phi}, \\ c &= \tilde{P}_3 \frac{1 - e^{-iu(1 + \sin\theta \cos\tilde{\phi})}}{1 + \sin\theta \cos\tilde{\phi}} + \tilde{P}_1 e^{-iu \sin\theta \cos\tilde{\phi}} \frac{1 - e^{-iu(1 - \sin\theta \cos\tilde{\phi})}}{1 - \sin\theta \cos\tilde{\phi}}.\end{aligned}\quad (28)$$

As discussed above, one does not specify the location of GW sources beforehand. Therefore, we carry out an average over the source locations and the polarization angles to obtain the all-sky averaged response function $R(u)$ as:

$$R(u) = \frac{1}{8\pi^2} \int_0^\pi \sin\theta d\theta \int_0^{2\pi} d\phi \int_0^{2\pi} d\psi (|F_+|^2 + |F_\times|^2).\quad (29)$$

The integration can be performed by first substituting the following relation

$$\begin{aligned}
 (\xi_{1,+})^2 + (\xi_{1,\times})^2 &= (1 - \sin^2\theta \sin^2\phi)^2, \\
 (\xi_{2,+})^2 + (\xi_{2,\times})^2 &= (1 - \sin^2\theta \cos^2\tilde{\phi})^2, \\
 (\xi_{3,+})^2 + (\xi_{3,\times})^2 &= (1 - \sin^2\theta \cos^2\phi)^2, \\
 \xi_{3,+}\xi_{1,+} + \xi_{3,\times}\xi_{1,\times} &= \left[(1 - \sin^2\theta \cos^2\phi)(1 - \sin^2\theta \sin^2\phi) - 2\cos^2\theta \cos^2\frac{\gamma}{2} \right], \\
 \xi_{3,+}\xi_{2,+} + \xi_{3,\times}\xi_{2,\times} &= \left[(1 - \sin^2\theta \cos^2\phi)(1 - \sin^2\theta \cos^2\tilde{\phi}) - 2\cos^2\theta \sin^2\gamma \right], \\
 \xi_{1,+}\xi_{2,+} + \xi_{1,\times}\xi_{2,\times} &= \left[(1 - \sin^2\theta \sin^2\phi)(1 - \sin^2\theta \cos^2\tilde{\phi}) - 2\cos^2\theta \cos^2\frac{\gamma}{2} \right],
 \end{aligned} \tag{30}$$

into Eq. (27). It is worth noting that the angular integral in question is factorized from the rest of the expression and can be carried out analytically. We relegate the detailed calculations to Appendix B, and present here the resultant analytic expression for the averaged response functions for an arbitrary TDI combination

$$R(u) = \frac{2}{4}C_1[\tilde{P}_i(u)] \times f_1(u) + C_2[\tilde{P}_i(u)] \times f_2(u) + \frac{3}{4}C_3[\tilde{P}_i(u)] \times f_3(u) - \frac{3}{4}C_4[\tilde{P}_i(u)] \times f_4(u) + \frac{1}{4}C_5[\tilde{P}_i(u)] \times f_5(u), \tag{31}$$

where

$$\begin{aligned}
 C_3[\tilde{P}_i(u)] &= \sum_{i=1}^3 \text{Re}[(\tilde{P}_i \tilde{P}_{i+1}^* + \tilde{P}_i \tilde{P}_{(i-1)'}^*)e^{iu}], \\
 C_4[\tilde{P}_i(u)] &= \sum_{i=1}^3 \text{Im}[(\tilde{P}_i \tilde{P}_{i+1}^* + \tilde{P}_i \tilde{P}_{(i-1)'}^*)e^{iu}], \\
 C_5[\tilde{P}_i(u)] &= \sum_{i=1}^3 \text{Re}[\tilde{P}_i \tilde{P}_i^* + \tilde{P}_i \tilde{P}_{(i-1)'}^*],
 \end{aligned} \tag{32}$$

and

$$\begin{aligned}
 f_1(u) &= \frac{4}{3} - \frac{2}{u^2} + \frac{\sin 2u}{u^3}, \\
 f_2(u) &= \frac{-u \cos u + \sin u}{u^3} - \frac{\cos u}{3}, \\
 f_3(u) &= \log \frac{4}{3} - \frac{5}{18} + \frac{-5 \sin u + 8 \sin 2u - 3 \sin 3u}{8u} - \frac{1}{3} \left(\frac{4 + 9 \cos u + 12 \cos 2u + \cos 3u}{8u^2} \right) \\
 &\quad + \frac{1}{3} \left(\frac{-5 \sin u + 8 \sin 2u + 5 \sin 3u}{8u^3} \right) + \text{Ci}3u - 2\text{Ci}2u + \text{Ci}u, \\
 f_4(u) &= \frac{-5 \cos u + 8 \cos 2u - 3 \cos 3u}{8u} + \frac{1}{3} \left(\frac{9 \sin u + 12 \sin 2u + \sin 3u}{8u^2} - \frac{8 + 5 \cos u - 8 \cos 2u - 5 \cos 3u}{8u^3} \right) \\
 &\quad + 2\text{Si}2u - \text{Si}3u - \text{Si}u, \\
 f_5(u) &= -\log 4 + \frac{7}{6} + \frac{11 \sin u - 4 \sin 2u}{4u} - \frac{10 + 5 \cos u - 2 \cos 2u}{4u^2} + \frac{5 \sin u + 4 \sin 2u}{4u^3} + 2(\text{Ci}2u - \text{Ci}u).
 \end{aligned} \tag{33}$$

Here, SinIntegral $\text{Si}(z) = \int_0^z \sin t/t dt$ and CosIntegral $\text{Ci}(z) = -\int_z^\infty \cos t/t dt$. By employing results given by Eq. (33), we plot $|\frac{f(u)}{u^2}|$ in Fig. 3 which shows the respective magnitudes of each terms contributing to the resultant expression.

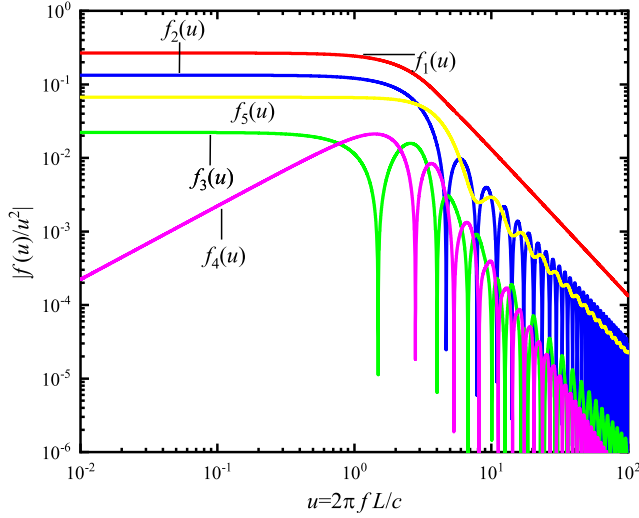


FIG. 3. The calculated individual contributions from each terms given in Eq. (33), $|\frac{f(u)}{u^2}|$, as functions of u .

It will also turn out to be useful to derive the asymptotical results at the low and high frequency limits. In the low frequency limit $u \ll 1$, we have

$$\begin{aligned} \text{Si}(2u) &\rightarrow 2u - \frac{4u^3}{9} + \frac{4u^5}{75} + o(u^7), \\ \text{Ci}(2u) &\rightarrow \ln(2u) + \gamma_E - u^2 + \frac{u^4}{6} - \frac{2u^6}{135} + o(u^8), \end{aligned} \quad (34)$$

where γ_E is the Euler constant. We therefore have

$$\begin{aligned} f_1(u) &\rightarrow \frac{4}{15}u^2 - \frac{8}{315}u^4 + o(u)^6, \\ f_2(u) &\rightarrow \frac{2}{15}u^2 - \frac{4}{315}u^4 + o(u)^6, \\ f_3(u) &\rightarrow -\frac{1}{45}u^2 + \frac{17}{1512}u^4 + o(u)^6, \\ f_4(u) &\rightarrow \frac{1}{45}u^3 - \frac{1}{315}u^5 + o(u)^6, \\ f_5(u) &\rightarrow -\frac{1}{15}u^2 + \frac{1}{2520}u^4 + o(u)^6. \end{aligned} \quad (35)$$

On the other hand, in the high frequency limit $u \gg 1$, one finds

$$\begin{aligned} \text{Si}(u) &\rightarrow \frac{\pi}{2} - \frac{\cos u}{u} + o\left(\frac{1}{u^2}\right), \\ \text{Ci}(u) &\rightarrow \frac{\sin u}{u} + o\left(\frac{1}{u^2}\right). \end{aligned} \quad (36)$$

Subsequently,

$$\begin{aligned} f_1(u) &\rightarrow \frac{4}{3} + o\left(\frac{1}{u^2}\right), \\ f_2(u) &\rightarrow -\frac{\cos u}{3} + o\left(\frac{1}{u^2}\right), \\ f_3(u) &\rightarrow \log \frac{4}{3} - \frac{5}{18} + \frac{3 \sin u}{8u} - \frac{\sin 3u}{24u} + o\left(\frac{1}{u^2}\right), \\ f_4(u) &\rightarrow \frac{3 \cos u}{8u} - \frac{\cos 3u}{24} + o\left(\frac{1}{u^2}\right), \\ f_5(u) &\rightarrow -\log 4 + \frac{7}{6} + \frac{\sin 2u}{2u} + \frac{3 \sin u}{4u} + o\left(\frac{1}{u^2}\right). \end{aligned} \quad (37)$$

The obtained asymptotic expressions will be utilized in the analysis of the sensitivity curves of specific TDI combinations below in Sec. IV.

Before proceeding to evaluate the SNR, let us revisit the particular case of the first-generation TDI Michelson combination X_1 . By substituting Eq. (8) into Eq. (32), one finds

$$\begin{aligned} C_1(u)_{X_1} &= 8(1 - \cos 2u), \\ C_2(u)_{X_1} &= 4(\cos u - \cos 3u), \\ C_3(u)_{X_1} &= 2(2 + 2 \cos 4u - 4 \cos 2u), \\ C_4(u)_{X_1} &= 2(2 \sin 4u - 4 \sin 2u), \\ C_5(u)_{X_1} &= 8(\cos 2u - 1). \end{aligned} \quad (38)$$

It can be further simplified to give

$$\begin{aligned} R(u) &= 2\sin^2 u \left[3 + 4 \log 2 - 6 \cos 2u \left(\log \frac{4}{3} - \frac{5}{18} \right) \right. \\ &\quad - \frac{8\cos^2 u}{3} - \frac{7 \sin u - 2 \sin 2u}{u} + \frac{5 \cos u - 8\cos^2 u}{u^2} \\ &\quad - \frac{5 \sin u - 4 \sin 2u}{u^3} - 4(\text{Ci}2u - \text{Ci}u) \\ &\quad - 6 \cos 2u(\text{Ci}3u - 2\text{Ci}2u + \text{Ci}u) \\ &\quad \left. - 6 \sin 2u(\text{Si}3u - 2\text{Si}2u + \text{Si}u) \right]. \end{aligned} \quad (39)$$

B. The signal-to-noise ratio and sensitivity function

The results obtained in the previous subsections furnish the necessary ingredients for obtaining the sensitivity function, which can be readily applied to the spaceborne detectors, such as LISA and TianQin. To proceed further, we note that Eq. (17) does not involve ψ . Therefore, for a monochromatic GW source, one may average out the inclination of the orbital plane and the polarization angle

to find the following expression for the PSD of the GW signal [20,22]

$$S_h(u) = \frac{2}{5}TH^2(|F_+|^2 + |F_\times|^2), \quad (40)$$

where T is the observation time, H is the GW strain. Subsequently, the SNR for the an arbitrary TDI combination in the frequency domain is given by

$$\text{SNR} \equiv \sqrt{\frac{S_h(u)}{N(u)}}. \quad (41)$$

By further averaging out the orientation and employing the result presented in the last subsection, one obtains the desired expression for the sensitivity function

$$S(u) \equiv 5 \frac{\sqrt{N(u)}}{\sqrt{\frac{2}{5}\sqrt{R(u)}}} \sqrt{\frac{1}{T}}, \quad (42)$$

where $T = 1$ year, 5 represents the SNR in an one-year observation period.

For the LISA mission, the armlength $L = 2.5 \times 10^6$ km. The corresponding ASDs of the TM and shot noises are, respectively, $s_a^{\text{LISA}} = 3 \times 10^{-15} \text{ ms}^{-2}/\sqrt{\text{Hz}}$ and $s_x^{\text{LISA}} = 20 \times 10^{-12} \text{ m}/\sqrt{\text{Hz}}$. While for TianQin, we have $L = 1.7 \times 10^5$ km, $s_a^{\text{TQ}} = 1 \times 10^{-15} \text{ ms}^{-2}/\sqrt{\text{Hz}}$ and $s_x^{\text{TQ}} = 1 \times 10^{-12} \text{ m}/\sqrt{\text{Hz}}$. Again, let us apply the above data to the specific example of Michelson X_1 combination. By using Eqs. (9), (39), and (42), the sensitivity curves of these

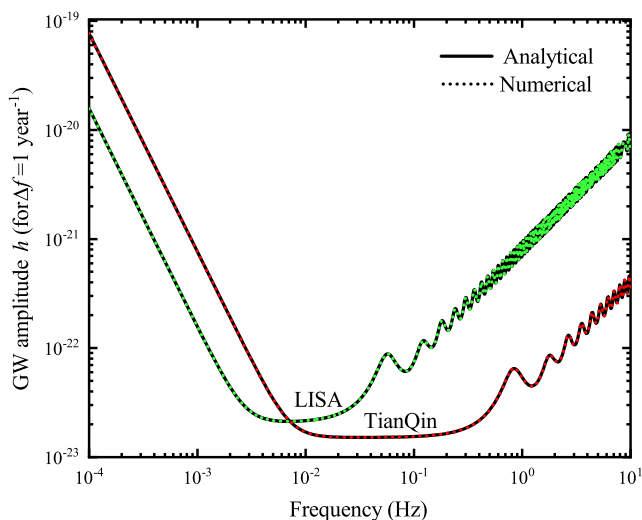


FIG. 4. Sensitivity curves of the spaceborne GW detectors LISA and TianQin, for the Michelson X_1 combination. The results obtained by analytic and numerical integration are shown in solid and dashed curves.

two missions are shown in Fig. 4. The analytic results are shown to be consistent with those obtained numerically by direct comparing against the latter in the plot. The figure demonstrates that the LISA mission is more sensitive to GW signals at the low frequency range, while TianQin is more involved for the signals with higher frequencies.

IV. FURTHER DISCUSSIONS

In this section, we analyze the asymptotic properties of the sensitivity functions for various TDI combinations. First, we focus on the difference observed between the six-link and eight-link TDI combination. Then, we explore the relevant properties of the optimal channel of specific TDI combinations.

A. Different asymptotic behaviors in the sensitivity curves between the six-link and eight-link TDI combination

The asymptotic behaviors of the sensitivity curves for the six-link and eight-link TDI combination in the low-frequency domain are known to be different. By taking the Sagnac combination α_1 and the Michelson combination X_1 as an example, this is demonstrated in Figs. 5 and 6. Although the inclinations of the curves on a logarithmic-logarithmic scale are the same, the curve for the Sagnac combination stays above that for Michelson one at small frequencies.

We show that this property can be readily understood by exploring the asymptotics of the respective sensitivity functions. For the X_1 combination, the analytical

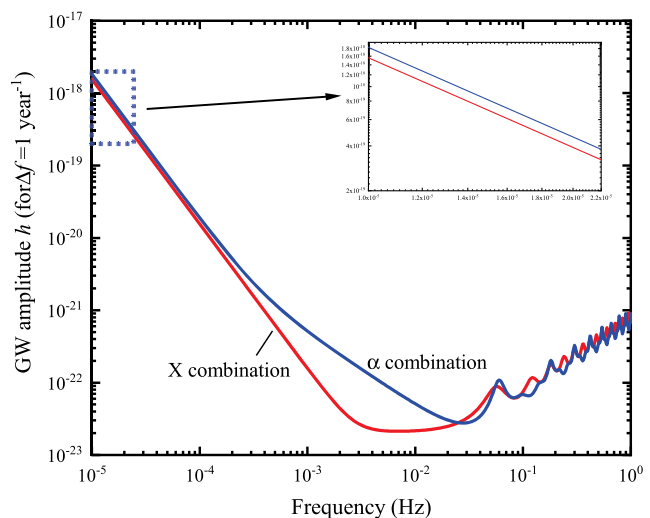


FIG. 5. The sensitivity curves of the Michelson and Sagnac combinations for the LISA mission ($\text{SNR} = 5$). The inset shows a zoom for the lower frequency region.

expressions of the sensitivity function are given by Eqs. (9), (39) and (42). On the other hand, for the Sagnac combination α_1 , the noise PSD is

$$N_{\alpha_1}(u) = 8 \frac{s_a^2 L^2}{u^2 c^4} \left(\sin^2 \frac{3}{2} u + 2 \sin^2 u \right) + 6 \frac{u^2 s_x^2}{L^2}, \quad (43)$$

while the coefficients of averaged response function read

$$\begin{aligned} C_1(u)_\alpha &= 6, \\ C_2(u)_\alpha &= -2(2 \cos 2u + 1), \\ C_3(u)_\alpha &= 8 + 4 \cos 3u, \\ C_4(u)_\alpha &= 4 \sin 3u, \\ C_5(u)_\alpha &= -4(2 \cos u + 1). \end{aligned} \quad (44)$$

The averaged response function can be further simplified to give

$$\begin{aligned} R(u) &= \frac{7}{6} + (2 + 4 \cos u) \log 2 + (6 + 3 \cos 3u) \log \frac{4}{3} \\ &+ \frac{-68 \sin u + 49 \sin 2u - 10 \sin 3u}{8u} - \cos u - \frac{\cos 3u}{6} \\ &+ \frac{-27 + 48 \cos u - 27 \cos 2u + 6 \cos 3u}{8u^2} - 4 \cos u (C_{i2u} - C_{iu}) \\ &+ \frac{-36 \sin u + 27 \sin 2u - 6 \sin 3u}{8u^3} + (6C_{i3u} - 14C_{i2u} + 8C_{iu}) \\ &+ 3 \cos 3u (C_{i3u} - 2C_{i2u} + C_{iu}) - 3 \sin 3u (2S_{i2u} - S_{i3u} - S_{iu}). \end{aligned} \quad (45)$$

By using the above expressions together with typical parameters for LISA and TianQin enumerated above, the resulting sensitive curves are shown in Figs. 5 and 6.

It is readily to show that, in the low frequency limit,

$$\begin{aligned} S(u)_X &\approx \frac{2}{u^2} \sqrt{\frac{10}{3}}, \\ S(u)_\alpha &\approx \frac{1}{u^2} \sqrt{\frac{55}{3}}. \end{aligned} \quad (46)$$

This serves to justify why at low frequencies, the slopes of two curves are identical while the Sagnac combination α_1 stays above that of the Michelson combination X_1 . In the high frequency limit,

$$\begin{aligned} S(u)_X &\approx 5 \sqrt{\frac{20 \frac{u^2 s_x^2}{L^2}}{\frac{5}{3} + 4 \log 2 - (6 \log \frac{4}{3} - \frac{1}{3}) \cos 2u}}, \\ S(u)_\alpha &\approx 5 \sqrt{\frac{15 \frac{u^2 s_x^2}{L^2}}{\frac{7}{6} + 2 \log 2 + 6 \log \frac{4}{3} + (2 \log 4 - 1) \cos u + (3 \log \frac{4}{3} - \frac{1}{6}) \cos 3u}}. \end{aligned} \quad (47)$$

The above formulae naturally explain the observed oscillations in these two combinations at the high frequency domain.

B. The optimum channel

All the TDI combinations and the corresponding optimal A , E , and T channels have been shown to possess rather different sensitivities properties. This is a consequence of their different response functions as well as system noises.

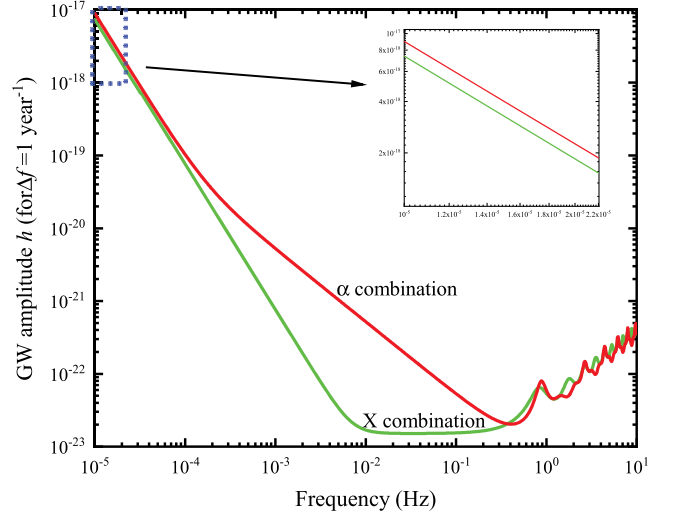


FIG. 6. The sensitivity curves of the Michelson and Sagnac combinations for the TianQin mission (SNR = 5). The inset shows a zoom for the lower frequency region.

Let us take Michelson combination as an example, the linear combinations of X, Y, Z constitute a group of optimal TDI channels, namely,

$$A = \frac{Z - X}{\sqrt{2}}, E = \frac{X - 2Y + Z}{\sqrt{6}}, T = \frac{X + Y + Z}{\sqrt{3}}. \quad (48)$$

The corresponding coefficients $P_i, P_{i'}$ of A, E, T channels are, respectively,

$$\begin{aligned} P_{1A} &= (1 - \mathcal{D}_{2'2}), P_{1'A} = (-1 - \mathcal{D}_2 + \mathcal{D}_{33'} + \mathcal{D}_{1'12}); \\ P_{2A} &= (\mathcal{D}_{1'} - \mathcal{D}_{22'1'}), P_{2'A} = (\mathcal{D}_3 - \mathcal{D}_{2'23}); \\ P_{3A} &= (-1 - \mathcal{D}_{2'} + \mathcal{D}_{1'1} + \mathcal{D}_{33'2'}), P_{3'A} = (1 - \mathcal{D}_{22'}), \end{aligned} \quad (49)$$

$$\begin{aligned} P_{1E} &= (-1 - 2\mathcal{D}_{3'} + \mathcal{D}_{2'2} + 2\mathcal{D}_{11'3'}), \\ P_{1'E} &= (1 - \mathcal{D}_2 - \mathcal{D}_{33'} + \mathcal{D}_{1'12}), \\ P_{2E} &= (2 + \mathcal{D}_{1'} - 2\mathcal{D}_{3'3} - \mathcal{D}_{22'1'}), \\ P_{2'E} &= (-2 - \mathcal{D}_3 + 2\mathcal{D}_{11'} + \mathcal{D}_{2'23}), \\ P_{3E} &= (-1 + \mathcal{D}_{2'} + \mathcal{D}_{1'1} - \mathcal{D}_{33'2'}), \\ P_{3'E} &= (1 + 2\mathcal{D}_1 - \mathcal{D}_{22'} - 2\mathcal{D}_{3'31}), \end{aligned} \quad (50)$$

and

$$\begin{aligned} P_{1T} &= (-1 + \mathcal{D}_{3'} + \mathcal{D}_{2'2} - \mathcal{D}_{11'3'}), \\ P_{1'T} &= (1 - \mathcal{D}_2 - \mathcal{D}_{33'} + \mathcal{D}_{1'12}), \\ P_{2T} &= (-1 + \mathcal{D}_{1'} + \mathcal{D}_{3'3} - \mathcal{D}_{22'1'}), \\ P_{2'T} &= (1 - \mathcal{D}_3 - \mathcal{D}_{11'} + \mathcal{D}_{2'23}), \\ P_{3T} &= (-1 + \mathcal{D}_{2'} + \mathcal{D}_{1'1} - \mathcal{D}_{33'2'}), \\ P_{3'T} &= (1 - \mathcal{D}_1 - \mathcal{D}_{22'} + \mathcal{D}_{3'31}). \end{aligned} \quad (51)$$

By employing the results in the previous section, the corresponding weights $f_j(u)$ can be obtained as follows:

$$\begin{aligned} C_1(u)_A &= 8(1 - \cos 2u)(2 + \cos u), \\ C_2(u)_A &= 8(1 - \cos 2u)(1 + 2\cos u), \\ C_3(u)_A &= 8(1 - \cos 2u)[1 - 2(\cos 2u + \cos u)], \\ C_4(u)_A &= 16(\cos 2u - 1)(\sin 2u + \sin u), \\ C_5(u)_A &= 8(\cos 2u - 1)(2\cos u + 1), \end{aligned} \quad (52)$$

$$\begin{aligned} C_1(u)_E &= 24(1 - \cos 2u)(2 + \cos u), \\ C_2(u)_E &= 24(1 - \cos 2u)(1 + 2\cos u), \\ C_3(u)_E &= 24(1 - \cos 2u)[1 - 2(\cos 2u + \cos u)], \\ C_4(u)_E &= 48(\cos 2u - 1)(\sin 2u + \sin u), \\ C_5(u)_E &= 24(\cos 2u - 1)(2\cos u + 1), \end{aligned} \quad (53)$$

and

$$\begin{aligned} C_1(u)_T &= 24(1 - \cos 2u)(1 - \cos u), \\ C_2(u)_T &= 24(1 - \cos 2u)(\cos u - 1), \\ C_3(u)_T &= 48(1 - \cos 2u)(1 - \cos u)\cos u, \\ C_4(u)_T &= 48(1 - \cos 2u)(1 - \cos u)\sin u, \\ C_5(u)_T &= 48(1 - \cos 2u)(\cos u - 1). \end{aligned} \quad (54)$$

Subsequently, the analytical expressions of the averaged response functions and the PSDs of the residual noise are found to be

$$\begin{aligned} 3R(u)_A = R(u)_E &= 2\sin^2 u \left\{ \frac{10}{3} + (18 - 12\cos u - 24\cos^2 u) \log \frac{4}{3} + (2 + 4\cos u) \log 4 + \frac{4}{3} \cos u (\cos u + 1) \right. \\ &+ \frac{-89\sin u + 28\sin 2u - \sin 3u}{4u} + \frac{-28 + 25\cos u - 28\cos 2u - 5\cos 3u}{4u^2} + \frac{-35\sin u + 28\sin 2u + 5\sin 3u}{4u^3} \\ &+ (18\text{Ci}3u - 40\text{Ci}2u + 22\text{Ci}u) - (12\cos u\text{Ci}3u - 16\cos u\text{Ci}2u + 4\cos u\text{Ci}u) + 12\sin u(2\text{Si}2u - \text{Si}3u - \text{Si}u) \\ &\left. + 24\cos u[\sin u(2\text{Si}2u - \text{Si}3u - \text{Si}u) - \cos u(\text{Ci}3u - 2\text{Ci}2u + \text{Ci}u)] \right\}, \end{aligned} \quad (55)$$

$$3N(u)_A = N(u)_E = 48\sin^2 u \left\{ [2(2 + \cos u) + 4(1 + 2\cos u)\cos u] \frac{s_a^2 L^2}{u^2 c^4} + (2 + \cos u) \frac{u^2 s_x^2}{L^2} \right\}, \quad (56)$$

$$\begin{aligned}
R(u)_T = 48\sin^2 u \sin^2 \frac{u}{2} & \left\{ \frac{1}{6} + 2 \log 2 - \frac{\cos u}{6} + 3 \cos u \log \frac{4}{3} \right. \\
& + \frac{2 \sin u - \sin 2u}{8u} + \frac{-5 + 10 \cos u - 5 \cos 2u}{8u^2} + \frac{5 \sin 2u - 10 \sin u}{8u^3} \\
& \left. - 2(\text{Ci}2u - \text{Ci}u) + 3 \cos u(\text{Ci}3u - 2\text{Ci}2u + \text{Ci}u) - 3 \sin u(2\text{Si}2u - \text{Si}3u - \text{Si}u) \right\}, \quad (57)
\end{aligned}$$

and

$$N(u)_T = 96\sin^2 u \sin^2 \frac{u}{2} \left[2(1 - 2 \cos u) \frac{s_a^2 L^2}{u^2 c^4} + \frac{u^2 s_x^2}{L^2} \right]. \quad (58)$$

The sensitivity curve for the optimum weighting of the data is given by [24]

$$S(u)_{\text{opt}} = 5h / \sqrt{\left(\frac{1}{S(u)_A}\right)^2 + \left(\frac{1}{S(u)_E}\right)^2 + \left(\frac{1}{S(u)_T}\right)^2}, \quad (59)$$

where the sensitivity functions $S(u)$ have been computed for a bandwidth of one cycle per year. It is noted that for the frequency range where the LISA and TianQin Michelson combination have the best sensitivity, the improvement in SNR for the optimal observable is slightly larger than $\sqrt{2}$.

By using Eqs. (5), (31), (42), and Eqs. (55)–(59), in Figs. 7–8, we plot the sensitivity curves of the LISA and TianQin missions for the optimal Michelson combination. It is observed that the sensitivity curves of A and E are identical across the entire band. In the long-wavelength region, the sensitivity of the channels A and E are more significant than that of the T model, whose contribution to the total SNR is negligible. At higher frequencies, however,

the sensitivity of the T channel turns out to be better or comparable to the other modes, and therefore it is mostly responsible for the improvement in SNR. We note that some of the above results have also been obtained in [24,43].

In Fig. 9 we plot the ratio between the optimal SNR and that of the Michelson combination for both the LISA and TianQin detectors. In the long-wavelength limit, the SNR is improved by a factor of $\sqrt{2}$. For Fourier frequencies equal to or greater than c/L , the improvement in SNR is in general appreciable but varies with the frequency. On average the improvement is about a factor of $\sqrt{3}$. In the

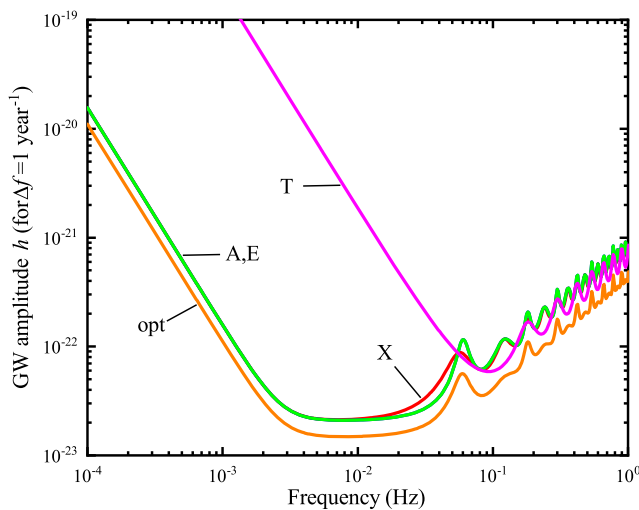


FIG. 7. The sensitivity curve of A , E , T , as well as the optimal combinations of the Michelson combination for the LISA detector (SNR = 5). The integration time is one year.

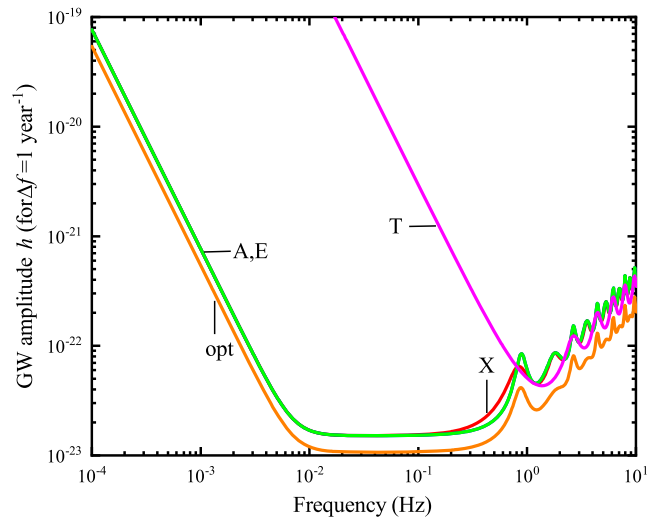


FIG. 8. The sensitivity curve of A , E , T , as well as the optimal combinations of the Michelson combination for the TianQin detector (SNR = 5). The integration time is one year.

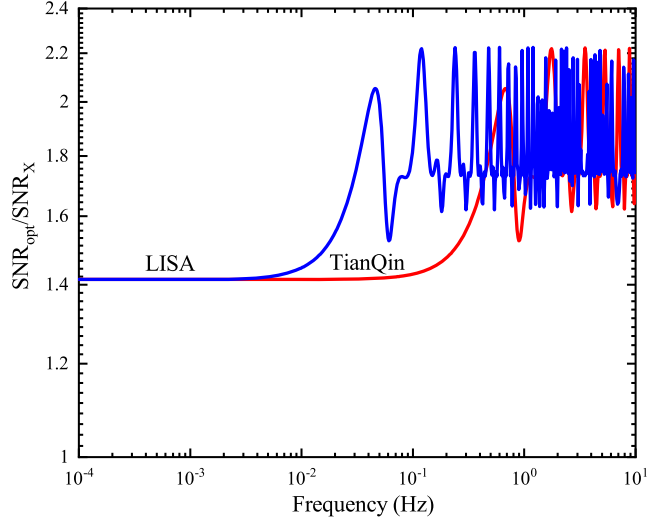


FIG. 9. The optimal SNR divided by the SNR of Michelson combination for LISA and TianQin detector, as a function of the Fourier frequency f . The sensitivity gain in the low-frequency band is equal to $\sqrt{2}$, while it can get larger than 2 at selected frequencies in the high-frequency region of the accessible band. The integration time has been assumed to be one year.

experimentally accessible band, for some specific frequencies, the factor may even attain the value of 2.

V. CONCLUDING REMARKS

In this work, we derive the analytical expressions of the sensitivity functions for the space-based interferometric GW detectors. The obtained results serve for any arbitrary TDI combination, which can be readily applied to those employed by LISA and TianQin missions. The main feature of our approach is that the angular average of the GW source can be factored out and the related integral can be performed analytically. A major advantage of the analytical formulas is that it offers a more efficient as well as accurate manner to evaluate the sensitivity curve. Moreover, it facilitates the investigation of the asymptotic properties of the relevant physical quantities in the low and high-frequency limits. In this regard, we discussed the reason behind the observed difference in the asymptotics of the sensitivity curves among various TDI combinations. The present approach is also utilized to derive the analytical results regarding the optimal channel. We argue that the results about the sensitivity curve obtained in the present study in on a rather general footing, which may be readily applied to any form of TDI combination. Also, it may potentially facilitate the relevant studies in the related topics.

ACKNOWLEDGMENTS

This work is supported by National Key RD Program of China (Grant No. 2020YFC2200500), Guangdong Major

project of Basic and Applied Basic Research (Grant No. 2019B030302001), the National Natural Science Foundation of China (Grants No. 11925503, No. 91636221, and No. 11805074), and the Fundamental Research Funds for the Central Universities, HUST: 2172019kfyRCPY029. We also acknowledge the financial support from Brazilian agencies Fundação de Amparo à Pesquisa do Estado de São Paulo (FAPESP), Fundação de Amparo à Pesquisa do Estado do Rio de Janeiro (FAPERJ), Conselho Nacional de Desenvolvimento Científico e Tecnológico (CNPq), Coordenação de Aperfeiçoamento de Pessoal de Nível Superior (CAPES).

APPENDIX A: THE POLYNOMIAL COEFFICIENTS FOR VARIOUS TDI COMBINATIONS

In this section, we list the coefficients of the polynomials of the form Eq. (2) for various TDI combinations.

1. Michelson combinations

For the first-generation Michelson combination X_1 , the relevant combination coefficients are

$$\begin{aligned} P_1 &= (\mathcal{D}_{2'2} - 1), P_{1'} = (1 - \mathcal{D}_{33'}), \\ P_2 &= 0, P_{2'} = (\mathcal{D}_{2'23} - \mathcal{D}_3), \\ P_3 &= (\mathcal{D}_{2'} - \mathcal{D}_{33'2}); P_{3'} = 0. \end{aligned} \quad (\text{A1})$$

For the second-generation X_2 , they are given by

$$\begin{aligned} P_1 &= -(1 - \mathcal{D}_{2'2} - \mathcal{D}_{2'233'} + \mathcal{D}_{33'2'22'2}), \\ P_{1'} &= (1 - \mathcal{D}_{33'} - \mathcal{D}_{33'2'2} + \mathcal{D}_{2'233'33'}), \\ P_2 &= 0, P_{2'} = -(1 - \mathcal{D}_{2'2} - \mathcal{D}_{2'233'} + \mathcal{D}_{33'2'22'2}), \\ P_3 &= (1 - \mathcal{D}_{33'} - \mathcal{D}_{33'2'2} + \mathcal{D}_{2'233'33'})\mathcal{D}_{2'}, P_{3'} = 0. \end{aligned} \quad (\text{A2})$$

2. Sagnac combinations

For the first-generation Sagnac combination α_1 , the coefficients read

$$\begin{aligned} P_1 &= 1, P_{1'} = -1, \\ P_2 &= \mathcal{D}_3, P_{2'} = -\mathcal{D}_{2'1'}, \\ P_3 &= \mathcal{D}_{31}, P_{3'} = -\mathcal{D}_{2'}. \end{aligned} \quad (\text{A3})$$

For the second-generation α_2 , they are given by

$$\begin{aligned} P_1 &= (1 - \mathcal{D}_{2'1'3'}), P_{1'} = -(1 - \mathcal{D}_{312}), \\ P_2 &= (1 - \mathcal{D}_{2'1'3'})\mathcal{D}_3, P_{2'} = -(1 - \mathcal{D}_{312})\mathcal{D}_{2'1'}, \\ P_3 &= (1 - \mathcal{D}_{2'1'3'})\mathcal{D}_{31}, P_{3'} = -(1 - \mathcal{D}_{312})\mathcal{D}_{2'}. \end{aligned} \quad (\text{A4})$$

3. Fully symmetric Sagnac combinations

For the first-generation fully symmetric Sagnac combination ζ_1 , the coefficients are

$$\begin{aligned} P_1 &= \mathcal{D}_1, P_{1'} = -\mathcal{D}_{1'}, \\ P_2 &= \mathcal{D}_2, P_{2'} = -\mathcal{D}_{2'}, \\ P_3 &= \mathcal{D}_3, P_{3'} = -\mathcal{D}_{3'}. \end{aligned} \quad (\text{A5})$$

For the second-generation ζ_2 , they are given by

$$\begin{aligned} P_1 &= \mathcal{D}_{11'} - \mathcal{D}_{2'3'1'}, P_{1'} = -(\mathcal{D}_{1'1} - \mathcal{D}_{321}), \\ P_2 &= (\mathcal{D}_{1'2'} - \mathcal{D}_{322'}), P_{2'} = -(\mathcal{D}_{1'2'} - \mathcal{D}_{322'}), \\ P_3 &= (\mathcal{D}_{13} - \mathcal{D}_{2'3'}), P_{3'} = -(\mathcal{D}_{13} - \mathcal{D}_{2'3'}). \end{aligned} \quad (\text{A6})$$

4. Beacon combinations

For the first-generation beacon combination B_1 , the coefficients read

$$\begin{aligned} P_1 &= 0, P_{1'} = 0, \\ P_2 &= -(\mathcal{D}_2 - \mathcal{D}_{3'1'}), P_{2'} = (\mathcal{D}_2 - \mathcal{D}_{11'2}), \\ P_3 &= -(\mathcal{D}_{3'} - \mathcal{D}_{11'3'}), P_{3'} = (\mathcal{D}_{3'} - \mathcal{D}_{21}). \end{aligned} \quad (\text{A7})$$

For the second-generation B_2 , they are given by

$$\begin{aligned} P_1 &= 0, P_{1'} = 0, \\ P_2 &= (\mathcal{D}_{3'22} - \mathcal{D}_{23'3'1'} - \mathcal{D}_{3'1'122} + \mathcal{D}_{211'3'3'1'}), \\ P_{2'} &= -(\mathcal{D}_{3'22} - \mathcal{D}_{3'2211'} - \mathcal{D}_{3'1'122} + \mathcal{D}_{3'1'12211'}), \\ P_3 &= (\mathcal{D}_{23'3'} - \mathcal{D}_{23'3'1'1} - \mathcal{D}_{211'3'3'} + \mathcal{D}_{211'3'3'1'1}), \\ P_{3'} &= -(\mathcal{D}_{23'3'} - \mathcal{D}_{21'13'3'} - \mathcal{D}_{3'221} + \mathcal{D}_{3'1'1221}). \end{aligned} \quad (\text{A8})$$

It is noted that in the literature, beacon combination is often denoted by the symbol “ P_i ”. In order to distinguish them from the polynomials of the delay operator, namely, P_i defined in Eq. (2), we have instead utilized “ B_i ”.

5. Monitor combinations

For the first-generation monitor combination E_1 , the coefficients are

$$\begin{aligned} P_1 &= -(1 - \mathcal{D}_{11'}), P_{1'} = (1 - \mathcal{D}_{11'}), \\ P_2 &= -(\mathcal{D}_3 - \mathcal{D}_{2'1'}), P_{2'} = 0, \\ P_3 &= 0, P_{3'} = (\mathcal{D}_{2'} - \mathcal{D}_{31}). \end{aligned} \quad (\text{A9})$$

For the second-generation E_2 , they are given by

$$\begin{aligned} P_1 &= -(1 - \mathcal{D}_{11'} - \mathcal{D}_{1'1} + \mathcal{D}_{11'1'1}), \\ P_{1'} &= (1 - \mathcal{D}_{1'1} - \mathcal{D}_{11'} + \mathcal{D}_{1'11'1}), \\ P_2 &= -(\mathcal{D}_3 - \mathcal{D}_{2'1'} - \mathcal{D}_{31'133} + \mathcal{D}_{2'11'2'2'1'}), P_{2'} = 0, \\ P_3 &= 0, P_{3'} = (\mathcal{D}_{2'} - \mathcal{D}_{31} - \mathcal{D}_{2'11'2'2'} + \mathcal{D}_{31'1331}). \end{aligned} \quad (\text{A10})$$

6. Relay combinations

For the first-generation relay combination U_1 , the coefficients are

$$\begin{aligned} P_1 &= 0, P_{1'} = -(\mathcal{D}_{3'} - \mathcal{D}_{11'3'}), \\ P_2 &= (1 - \mathcal{D}_{3'2'1'}), P_{2'} = -(1 - \mathcal{D}_{11'}), \\ P_3 &= 0, P_{3'} = (\mathcal{D}_1 - \mathcal{D}_{3'2'}). \end{aligned} \quad (\text{A11})$$

For the second-generation U_2 , they are given by

$$\begin{aligned} P_1 &= 0, P_{1'} = -(\mathcal{D}_{13'} - \mathcal{D}_{11'3'2'3'} - \mathcal{D}_{111'3'} + \mathcal{D}_{3'2'1'111'3'}), \\ P_2 &= (\mathcal{D}_1 - \mathcal{D}_{11'3'2'} - \mathcal{D}_{13'2'1'} + \mathcal{D}_{11'3'2'3'2'1'}), \\ P_{2'} &= -(\mathcal{D}_1 - \mathcal{D}_{111'} - \mathcal{D}_{11'3'2'} + \mathcal{D}_{3'2'1'111'}), \\ P_3 &= 0, P_{3'} = (\mathcal{D}_{11} - \mathcal{D}_{13'2'} - \mathcal{D}_{3'2'1'11} + \mathcal{D}_{11'3'2'3'2'}). \end{aligned} \quad (\text{A12})$$

APPENDIX B: ANGULAR AVERAGE IN THE CALCULATION OF THE RESPONSE FUNCTION OF THE SIGNAL

This appendix provides a detailed derivation of the averaged response function of the GW signal. From Eqs. (27) and (30), we have

$$4(|F_+|^2 + |F_\times|^2) = n_1(u, \theta, \phi, \gamma) + n_2(u, \theta, \phi, \gamma) + n_3(u, \theta, \phi, \gamma) + n_4(u, \theta, \phi, \gamma) + n_5(u, \theta, \phi, \gamma) + n_6(u, \theta, \phi, \gamma), \quad (\text{B1})$$

where

$$\begin{aligned} n_1(u, \theta, \phi, \gamma) &= |a|^2(1 - \sin^2\theta\cos^2\phi)^2, \\ n_2(u, \theta, \phi, \gamma) &= |b|^2(1 - \sin^2\theta\sin^2\phi)^2, \\ n_3(u, \theta, \phi, \gamma) &= |c|^2(1 - \sin^2\theta\cos^2\tilde{\phi})^2, \end{aligned}$$

$$\begin{aligned}
 n_4(u, \theta, \phi, \gamma) &= 2\text{Re}(ab^*) \times \left[(1 - \sin^2\theta \cos^2\phi)(1 - \sin^2\theta \sin^2\phi) - 2\cos^2\theta \cos^2\frac{\gamma}{2} \right], \\
 n_5(u, \theta, \phi, \gamma) &= 2\text{Re}(ac^*) \times \left[(1 - \sin^2\theta \cos^2\phi)(1 - \sin^2\theta \cos^2\tilde{\phi}) - 2\cos^2\theta \sin^2\gamma \right], \\
 n_6(u, \theta, \phi, \gamma) &= 2\text{Re}(bc^*) \times \left[(1 - \sin^2\theta \sin^2\phi)(1 - \sin^2\theta \cos^2\tilde{\phi}) - 2\cos^2\theta \cos^2\frac{\gamma}{2} \right].
 \end{aligned} \tag{B2}$$

The integration with respect to the angles (θ, ϕ) for the entire solid angle, as given by Eq. (29), leads to

$$\begin{aligned}
 &\frac{1}{4\pi} \int_0^\pi \sin\theta d\theta \int_0^{2\pi} d\phi (|F_+|^2 + |F_\times|^2) \\
 &= \frac{2}{4} C_1[\tilde{P}_i(u)] \times f_1(u) + C_2[\tilde{P}_i(u)] \times f_2(u) + \frac{3}{4} C_3[\tilde{P}_i(u)] \times f_3(u) - \frac{3}{4} C_4[\tilde{P}_i(u)] \times f_4(u) + \frac{1}{4} C_5[\tilde{P}_i(u)] \times f_5(u),
 \end{aligned} \tag{B3}$$

where

$$\begin{aligned}
 f_1(u) &= \frac{1}{4\pi} \int_0^\pi \sin\theta d\theta \int_0^{2\pi} d\phi \left\{ \frac{4}{3} - \cos u \cos(u \sin\theta \cos\phi) \left[1 + \frac{\sin^2\theta}{2} (1 + \cos 2\phi) \right] \right. \\
 &\quad \left. - 2 \sin u \sin(u \sin\theta \cos\phi) \sin\theta \cos\phi \right\}, \\
 f_2(u) &= \frac{1}{4\pi} \int_0^\pi \sin\theta d\theta \int_0^{2\pi} d\phi \left\{ \cos(u \sin\theta \cos\phi) \left[1 - \frac{\sin^2\theta}{2} (1 + \cos 2\phi) \right] - \cos u \frac{2}{3} \right\}, \\
 f_3(u) - if_4(u) &= \frac{1}{4\pi} \int_0^\pi \sin\theta d\theta \int_0^{2\pi} d\phi \\
 &\quad \times \left[\frac{\frac{3}{2} e^{iu} - 2e^{-iu \sin\theta \cos\phi} + e^{-iu(1 + \sin\theta(\cos\phi - \cos\tilde{\phi}))}}{(1 + \sin\theta \cos\phi)(1 - \sin\theta \cos\tilde{\phi})} \times \cos^2\theta \right. \\
 &\quad \left. + \frac{1}{3} \left[e^{iu} - 2e^{iu \sin\theta \cos\phi} + e^{-iu(1 - \sin\theta(\cos\phi - \cos\tilde{\phi}))} \right] (1 + \sin\theta \cos\phi)(1 - \sin\theta \cos\tilde{\phi}) \right], \\
 f_5(u) &= \frac{1}{4\pi} \int_0^\pi \sin\theta d\theta \int_0^{2\pi} d\phi \\
 &\quad \times \left[\frac{\frac{3}{2} \frac{1 - 2 \cos[u(1 + \sin\theta \cos\phi)] + e^{iu \sin\theta(\cos\phi - \cos\tilde{\phi})}}{(1 + \sin\theta \cos\phi)(1 + \sin\theta \cos\tilde{\phi})} \times \cos^2\theta \right. \\
 &\quad \left. - \frac{1}{3} \left(1 - 2 \cos[u(1 - \sin\theta \cos\phi)] + e^{-iu \sin\theta(\cos\phi - \cos\tilde{\phi})} \right) (1 + \sin\theta \cos\phi)(1 + \sin\theta \cos\tilde{\phi}) \right].
 \end{aligned} \tag{B4}$$

First, $f_1(u)$ and $f_2(u)$ only involve the ordinary integrals of trigonometric functions and thus can be evaluated straightforwardly to give

$$\begin{aligned}
 f_1(u) &= \left(\frac{4}{3} - \frac{2}{u^2} + \frac{\sin 2u}{u^3} \right), \\
 f_2(u) &= \left(\frac{-u \cos u + \sin u}{u^3} - \frac{\cos u}{3} \right).
 \end{aligned} \tag{B5}$$

The integral in $f_3(u)$, $f_4(u)$ and $f_5(u)$ can be simplified by appropriately introducing a change of variables. To be specific, one adapts

$$\begin{aligned}
 x &= \sin\theta \cos\phi = \frac{(\tilde{x} + \tilde{y})}{\sqrt{3}}, \\
 y &= \sin\theta \sin\phi = \tilde{x} - \tilde{y}.
 \end{aligned} \tag{B6}$$

The above definitions can be viewed as transforming from region of a unit hemispherical surface $[\theta \in (0, \pi/2), \phi \in (0, 2\pi)]$ to that of a circular surface $x^2 + y^2 \leq 1$. Then one further stretches the circle into an ellipse, namely,

$$\begin{aligned}
 \tilde{x} &= \sin\theta \cos\phi = x \frac{\sqrt{3}}{2} + y \frac{1}{2}, \\
 \tilde{y} &= \sin\theta \sin\phi = x \frac{\sqrt{3}}{2} - y \frac{1}{2}.
 \end{aligned} \tag{B7}$$

As a result, the initial integration on the unit hemispherical surface becomes an elliptic one, bounded by the equation

$\frac{4}{3}(\tilde{x}^2 + \tilde{y}^2 - \tilde{x}\tilde{y}) \leq 1$. It is also noted the Jacobian determinant of the transformation reads

$$d\tilde{x}d\tilde{y} = \frac{\sqrt{3}}{2} \sin\theta \cos\theta d\theta d\phi. \quad (\text{B8})$$

Subsequently, the integration gives

$$\begin{aligned} & \frac{1}{4\pi} \int_0^\pi \sin\theta d\theta \int_{-\pi}^\pi d\phi \frac{\cos(u \sin\theta \cos\phi) \cos^2\theta}{(1 + \sin\theta \cos\phi)(1 + \sin\theta \cos\tilde{\phi})} \\ &= \frac{2}{3\pi} \int_{-1}^1 d\tilde{x} \frac{\cos(u\tilde{x})}{1 + \tilde{x}} \int_{\frac{\tilde{x}-\sqrt{3}\sqrt{1-\tilde{x}^2}}{2}}^{\frac{\tilde{x}+\sqrt{3}\sqrt{1-\tilde{x}^2}}{2}} d\tilde{y} \frac{\sqrt{\frac{3}{4}(1-\tilde{x}^2) - (\tilde{y} - \frac{\tilde{x}}{2})^2}}{1 + \tilde{y}} \end{aligned} \quad (\text{B9})$$

$$\begin{aligned} &= \frac{1}{u} \left(\sin u - \sin \frac{u}{2} \right) - \frac{1}{3u} \left(\sin u + \sin \frac{u}{2} \right) \\ &+ \frac{2}{3} \left[\cos u \left(\text{Ci}2u - \text{Ci} \frac{u}{2} \right) + \sin u \left(\text{Si}2u - \text{Si} \frac{u}{2} \right) \right]. \end{aligned} \quad (\text{B10})$$

Alternatively, if one assumes $\tilde{x} = \frac{x+y}{\sqrt{2}}, \tilde{y} = \frac{x-y}{\sqrt{2}}$, the oblique ellipse plane equation $\tilde{x}^2 + \tilde{y}^2 - \tilde{x}\tilde{y} - \frac{3}{4} = 0$ becomes $\frac{x^2}{\frac{3}{2}} + \frac{y^2}{\frac{3}{2}} = 1$. In this case, one has

$$\begin{aligned} & \frac{1}{4\pi} \int_0^\pi \sin\theta d\theta \int_{-\pi}^\pi d\phi \frac{\cos(u \sin\theta (\cos\phi - \cos\tilde{\phi})) \cos^2\theta}{(1 + \sin\theta \cos\phi)(1 + \sin\theta \cos\tilde{\phi})} \\ &= \frac{2}{3\pi} \frac{\sqrt{\frac{3}{4} - \tilde{x}^2 - \tilde{y}^2 + \tilde{x}\tilde{y}} \cos[u(\tilde{x} - \tilde{y})]}{(1 + \tilde{x})(1 + \tilde{y})} \\ &= \frac{2}{3\pi} \frac{\sqrt{\frac{3}{4} - \frac{x^2}{2} - \frac{3y^2}{2}} \cos(\sqrt{2}uy)}{1 + \sqrt{2}x + \frac{x^2-y^2}{2}} \\ &= -\frac{4 \sin u}{3u} + \frac{4}{3u} 2 \sin \frac{u}{2} + \frac{4}{3} \left(\text{Ci}u - \text{Ci} \frac{u}{2} \right). \end{aligned} \quad (\text{B11})$$

The above results can be utilized to obtain the desired expressions of $f_j(u)$ given in Eq. (33).

-
- [1] B. Abbott *et al.* (LIGO Scientific and Virgo Collaborations), *Phys. Rev. Lett.* **116**, 061102 (2016).
- [2] B. P. Abbott *et al.* (LIGO Scientific and Virgo Collaborations), *Phys. Rev. Lett.* **116**, 241103 (2016).
- [3] B. P. Abbott *et al.* (LIGO Scientific and VIRGO Collaborations), *Phys. Rev. Lett.* **118**, 221101 (2017); **121**, 129901 (E) (2018).
- [4] B. Abbott *et al.* (LIGO Scientific and Virgo Collaborations), *Phys. Rev. Lett.* **119**, 161101 (2017).
- [5] B. Abbott *et al.* (LIGO Scientific and Virgo Collaborations), *Phys. Rev. Lett.* **119**, 141101 (2017).
- [6] B. P. Abbott *et al.* (LIGO Scientific and Virgo Collaborations), *Astrophys. J. Lett.* **851**, L16 (2017).
- [7] B. Abbott *et al.* (LIGO Scientific and Virgo Collaborations), *Phys. Rev. X* **9**, 031040 (2019).
- [8] J. Aasi *et al.* (LIGO Scientific Collaboration), *Classical Quantum Gravity* **32**, 074001 (2015).
- [9] F. Acernese *et al.* (VIRGO Collaboration), *Classical Quantum Gravity* **32**, 024001 (2015).
- [10] S. Kawamura *et al.*, *Classical Quantum Gravity* **23**, S125 (2006).
- [11] P. Amaro-Seoane *et al.* (LISA Collaboration), [arXiv:1702.00786](https://arxiv.org/abs/1702.00786).
- [12] W.-T. Ni, *Int. J. Mod. Phys. D* **22**, 1341004 (2013).
- [13] TianQin, J. Luo *et al.*, *Classical Quantum Gravity* **33**, 035010 (2016).
- [14] X. Gong *et al.*, *J. Phys. Conf. Ser.* **610**, 012011 (2015).
- [15] K. Somiya (KAGRA Collaboration), *Classical Quantum Gravity* **29**, 124007 (2012).
- [16] W.-T. Ni, *Int. J. Mod. Phys. D* **11**, 947 (2002).
- [17] B. Hiscock and R. W. Hellings, *Bull. Am. Astron. Soc.* **29**, 1312 (1997), <http://articles.adsabs.harvard.edu/pdf/1997BAAS...29.1312H.4>.
- [18] G. Hobbs *et al.*, *Pub. Astron. Soc. Aust.* **26**, 103 (2009).
- [19] S. L. Larson, W. A. Hiscock, and R. W. Hellings, *Phys. Rev. D* **62**, 062001 (2000).
- [20] M. Vallisneri, J. Crowder, and M. Tinto, *Classical Quantum Gravity* **25**, 065005 (2008).
- [21] N. J. Cornish and L. J. Rubbo, *Phys. Rev. D* **67**, 022001 (2003); **67**, 029905(E) (2003).
- [22] M. Vallisneri and C. R. Galley, *Classical Quantum Gravity* **29**, 124015 (2012).
- [23] M. Tinto and J. Armstrong, *Phys. Rev. D* **59**, 102003 (1999).
- [24] M. Tinto and S. V. Dhurandhar, *Living Rev. Relativity* **24**, 1 (2021).
- [25] D. A. Shaddock, M. Tinto, F. B. Estabrook, and J. Armstrong, *Phys. Rev. D* **68**, 061303 (2003).

- [26] M. Vallisneri, *Phys. Rev. D* **72**, 042003 (2005); **76**, 109903 (E) (2007).
- [27] M. Muratore, D. Vetrugno, and S. Vitale, *Classical Quantum Gravity* **37**, 185019 (2020).
- [28] S. L. Larson, R. W. Hellings, and W. A. Hiscock, *Phys. Rev. D* **66**, 062001 (2002).
- [29] C. Zhang, Q. Gao, Y. Gong, D. Liang, A. J. Weinstein, and C. Zhang, *Phys. Rev. D* **100**, 064033 (2019).
- [30] A. Blaut, *Phys. Rev. D* **85**, 043005 (2012).
- [31] M. Tinto and M. E. da Silva Alves, *Phys. Rev. D* **82**, 122003 (2010).
- [32] X.-Y. Lu, Y.-J. Tan, and C.-G. Shao, *Phys. Rev. D* **100**, 044042 (2019).
- [33] M. Tinto and O. Hartwig, *Phys. Rev. D* **98**, 042003 (2018).
- [34] O. Hartwig and J.-B. Bayle, [arXiv:2005.02430](https://arxiv.org/abs/2005.02430).
- [35] L. S. S. Team, *Laser Interferometer Space Antenna: A Cornerstone Mission for the Observation of Gravitational Waves*, ESA System and Technology Study Report ESA-SCI 11 (European Space Agency, France, 2000).
- [36] J. Sylvestre and M. Tinto, *Phys. Rev. D* **68**, 102002 (2003).
- [37] S. Dhurandhar, K. Rajesh Nayak, and J. Vinet, *Phys. Rev. D* **65**, 102002 (2002).
- [38] A. Petiteau, G. Auger, H. Halloin, O. Jeannin, E. Plagnol, S. Pireaux, T. Regimbau, and J.-Y. Vinet, *Phys. Rev. D* **77**, 023002 (2008).
- [39] F. B. Estabrook, M. Tinto, and J. W. Armstrong, *Phys. Rev. D* **62**, 042002 (2000).
- [40] N. J. Cornish, *Phys. Rev. D* **65**, 022004 (2001).
- [41] M. Tinto, F. B. Estabrook, and J. W. Armstrong, *Phys. Rev. D* **65**, 082003 (2002).
- [42] L. J. Rubbo, N. J. Cornish, and O. Poujade, *Phys. Rev. D* **69**, 082003 (2004).
- [43] K. Nayak, A. Pai, S. Dhurandhar, and J.-Y. Vinet, *Classical Quantum Gravity* **20**, 1217 (2003).